Arctic Ocean Radiative Fluxes and Cloud Forcing Estimated from the ISCCP C2 Cloud Dataset, 1983–1990

AXEL J. SCHWEIGER

Polar Science Center, Applied Physics Laboratory, University of Washington, Seattle, Washington

JEFFREY R. KEY

Cooperative Institute for Research in Environmental Sciences, Division of Cryospheric and Polar Processes, University of Colorado, Boulder, Colorado

(Manuscript received 30 June 1993, in final form 15 November 1993)

ABSTRACT

Radiative fluxes and cloud forcings for the ocean areas of the Arctic are computed from the monthly cloud product of the International Satellite Cloud Climatology Project (ISCCP) for 1983–90. Spatially averaged shortwave fluxes compare well with climatological values, while downwelling longwave fluxes are significantly lower. This is probably due to the fact that the ISCCP cloud amounts are underestimates. Top-of-the-atmosphere radiative fluxes are in excellent agreement with measurements from the Earth Radiation Budget Experiment (ERBE). Computed cloud forcings indicate that clouds have a warming effect at the surface and at the top of the atmosphere during winter and a cooling effect during summer. The net radiative effect of clouds is larger at the surface during winter but greater at the top of the atmosphere during summer. Overall the net radiative effect of clouds at the top of the atmosphere is one of cooling. This is in contrast to a previous result from ERBE data showing that arctic cloud forcings have a net warming effect. Sensitivities to errors in input parameters are generally greater during winter with cloud amount being the most important parameter. During summer the surface radiation balance is most sensitive to errors in the measurements of surface reflectance.

The results are encouraging, but the estimated error of 20 W m^{-2} in surface net radiative fluxes is too large, given that estimates of the net radiative warming effect due to a doubling of CO_2 are on the order of 4 W m^{-2}. Because it is difficult to determine the accuracy of results with existing in situ observations, it is recommended that the development of improved algorithms for the retrieval of surface radiative properties be accompanied by the simultaneous assembly of validation datasets.

1. Introduction

The most comprehensive compilations of information on arctic radiative fluxes are nearly 30 years old. The climatologies of Marshunova (1961; Marshunova and Chernigovsky 1966) and Vowinckel and Orvig (1962, 1963, 1964) are based on information from a sparse network of drifting stations, ice islands, and coastal stations. Although some of the coastal stations have provided reliable long-term records of radiation balance components (Ohmura and Gilgen 1991) for the ice-covered areas of the Arctic Ocean, these climatologies rely on drifting stations records with highly variable temporal and spatial deployment histories. Further, drifting stations are generally established on large multiyear ice floes or ice islands, and measurements there will be more representative of thick ice where the energy fluxes through the ice are small (Makshtas 1991).

The problem of the spatial representativeness of drifting station measurements is particularly severe with respect to surface albedo, which becomes highly variable during summer due to the development of melt ponds, and in the marginal seas where there is a broad range of ice concentrations. Similar problems exist for the interpolation of surface temperatures that depend on distribution of ice thickness and open water areas. In their compilation of arctic radiative fluxes Vowinckel and Orvig (1962) have addressed this problem by using surface albedos weighted by ice concentration (Larson and Orvig 1962). However, their ice concentration data, a compilation from the *Oceanographic Atlas of the Polar Seas* (U.S. Navy 1958) and various sources from the Deutsches Hydrographisches Institut (1950), are of questionable quality. Fletcher (1966) reviewed the information then available on radiative fluxes. He questions Gavrilova's (1966) estimates that total solar radiation in the Arctic is known to an accuracy of 2.5% for annual fluxes, 5%–10% for monthly fluxes, absorbed solar radiation to 10%–15%, outgoing longwave to 15%–20%, and the radiation balance to 20%–30%, noting that differences between

Corresponding author address: Dr. Axel J. Schweiger, Applied Physics Laboratory, 1013 NE 40th Street, Seattle, WA 98105-6698.

Marshunova's and Vowinckel and Orvig's climatologies are much greater than the estimated accuracies. Fletcher concluded that the compilation of Marshunova (1961) probably represented the most accurate description of the radiation climate in the Arctic. Ohmura (1981) arrived at the same conclusion 15 years later.

While the Marshunova climatology may indeed represent the general characteristics of the radiation climate in the Arctic, the information in that dataset is of limited utility, in part for the above reasons, and in part because of its low spatial resolution. The record from Russian drifting stations continues until today (Colony et al. 1992) but has not been processed into a comprehensive climatology. Even such an extended climatology will suffer from the biases and shortcomings related to the lack of spatial representativeness. Although it would be valuable for climate monitoring, it will be of limited utility for sea-ice modeling experiments and validation of general circulation models. For such applications, datasets of radiative fluxes derived using remote sensing techniques, possibly in combination with surface measurements, will have to be developed. This need for development and validation of datasets of surface radiation balance components derived from satellite was clearly identified by the World Climate Research Programme (WMO 1992).

The objective of our study is the compilation of a monthly climatology of arctic radiative fluxes at the surface as well as at the top of the atmosphere. The term *climatology* is used somewhat loosely in this context since it covers only seven years. This compilation provides an alternative to prior estimates. It incorporates the most recent satellite-derived datasets, which for the first time allow the investigation of the spatial variability of arctic radiative fluxes. These fluxes are computed using a radiative transfer modeling approach, with the International Satellite Cloud Climatology Project (ISCCP) C2 dataset as the main source of information on radiatively important atmospheric and surface properties. Due to the limitations of satellite remote sensing retrieval techniques, a secondary objective of this study is to determine the range of errors that we may expect owing to deficiencies in the input dataset.

2. ISCCP C2 data description and comparison with surface observations

Radiative fluxes are computed using the ISCCP C2 dataset as the primary source of information for radiatively important atmospheric and surface properties. The C2 set is a compilation of monthly statistics from the 3-h ISCCP C1 dataset and contains information on satellite-derived cloud fraction, atmospheric profiles of temperature, water vapor and ozone, surface temperature and reflectivity, cloud-top pressure and temperature, and cloud optical depth. Compilation is an ongoing effort; currently available data cover the period from July 1983 to December 1990. This dataset provides global coverage from a variety of sensors on a 280 km × 280 km analysis grid. For the polar regions it consists entirely of data from the Advanced Very High Resolution Radiometer (AVHRR) and *TIROS-N* Operational Vertical Sounder (TOVS) on board the National Oceanic and Atmospheric Administration (NOAA) satellites. The ISCCP procedure involves a large number of processing steps; for more detail the reader is referred to Rossow et al. (1991). Data covering all ocean areas north of 62.5°N from 1983 through 1990 are used in the analysis.

Since the radiative fluxes presented here are based upon the ISCCP cloud amounts, the validity of those amounts should be examined. We do so here by comparing the satellite-based cloud amounts with surface-based observations. However, there are many questions concerning the validity of the surface-based cloud amounts as well, so it is not possible to draw conclusions in an absolute sense about either dataset. Only a summary of the results is presented here; for more details see Schweiger and Key (1992).

The comparison is made with monthly cloud statistics from an atlas of global cloud cover compiled by Warren et al. (1988; hereafter WAR). Cloud observations from ships for 1951–81 form the basis for the ocean area atlas. Since there is no direct overlap between the ISCCP and WAR datasets, only monthly statistics were compared. Interannual variability of monthly cloudiness is small, in the range of 5% for July and up to 8% in January of the ISCCP years, so errors due to nonoverlapping climatologies should be of lower magnitude than the other potential error sources.

Figure 1 shows the annual variation of total cloud amounts in the ISCCP C2 and WAR datasets for the region north of 62.5°N, including land areas. Two separate cloud amounts are given for the ISCCP C2 set: the total cloud amount reported in the ISCCP C2 dataset and marginal cloud amount. (The total cloud includes the marginal cloud.) Marginal cloud amounts are derived in the ISCCP procedure through the application of a different threshold and represent the first derivative of cloud amount with respect to the threshold. These marginally cloudy pixels display radiances that are near the clear-sky radiances. The marginal cloud amount is presented as an indicator of the level of uncertainty in the thresholds. As can be seen from Fig. 1, the uncertainty is greatest during winter.

The satellite cloud amounts are generally 5%–35% less than the surface observations over the entire Arctic. Regional differences may be as high as 45%, however. In winter the ISCCP climatology in the central Arctic

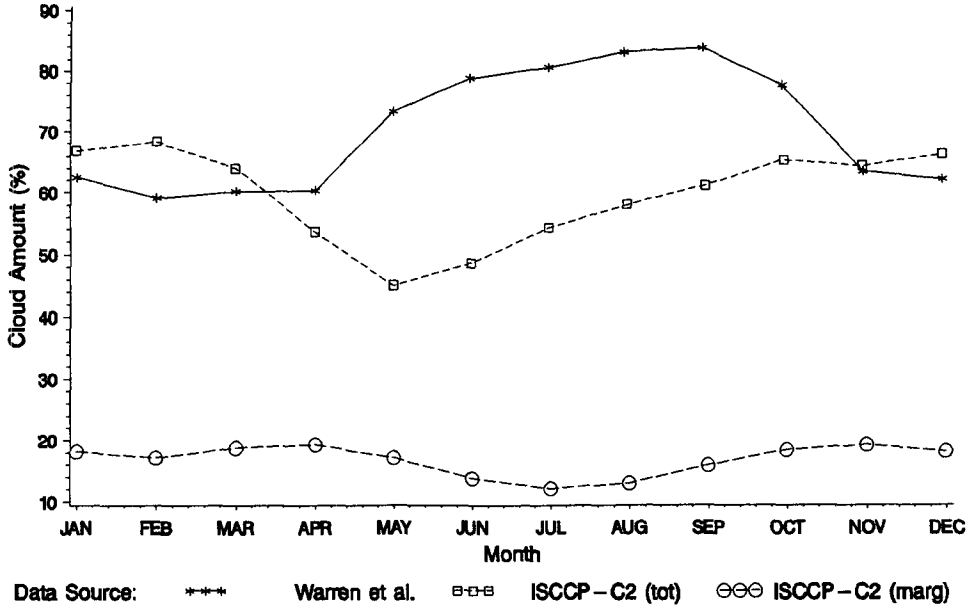

FIG. 1. Cloud amounts from the ISCCP C2 dataset for the period 1983–90 and from the Warren et al. dataset for the period 1951–81. Marginal cloud amounts from the ISCCP dataset are also shown.

agrees within 10% of the surface observations. Satellite-derived cloudiness during summer seems to reflect the conservative approach of the ISCCP algorithm and probably represents an underestimate, but there is considerable uncertainty with respect to the winter cloudiness. Ice crystal precipitation could account for the unexpectedly high winter ISCCP cloud amounts (Schweiger and Key 1992).

3. Calculation of radiative fluxes

A review of techniques to infer surface radiative fluxes from top-of-the-atmosphere (TOA) radiances is provided by Schmetz (1989) and Raschke et al. (1992), who also discuss the application of such techniques to the polar regions. Median rms errors of satellite-derived solar fluxes for lower latitudes are near 5% for monthly sums, near 9% for daily sums, and 5%–50% for hourly sums (Schmetz 1989). Rossow and Lacis (1990) use NOAA scanning radiometer (SR) data to compute the surface radiation balance globally for 4 months in 1977, but problems in the polar regions are not specifically addressed. Using data from the ISCCP project, Rossow et al. (1990) computed radiative flux profiles and compared them to surface measurements in Wisconsin and Bermuda. Their results are encouraging since they showed rms errors of 4 and 9 W m^{-2}, respectively, in downwelling solar radiation for the two areas. To date, only a small number of case studies have been conducted in the polar regions. Using surface and aircraft measurements from the Fram Strait area during the Arktis-88 experiment, Stuhlmann and Bauer (1991) found that satellite-derived solar irradiances were underestimated by 30–50 W m^{-2}, or 10%. They found these errors to be particularly large near the ice edge where the resolution of the AVHRR sensor is insufficient to distinguish ice-free and ice-covered areas. Satellite-retrieved surface albedos were lower by up to 0.2 than those measured on the ground, which contributed to the error in downwelling shortwave fluxes. This underestimation of surface albedo was attributed mainly to the different scales of areal integration. Combining a discrete-ordinate radiative transfer model (Stamnes et al. 1988) for the inversion of satellite radiances to cloud transmissivities and a two-stream model for the calculation of radiative fluxes at the surface, Kergormard et al. (1993) found a ± 10 W m^{-2} agreement between satellite-retrieved fluxes and those measured on board a ship in Fram Strait on 31 August 1988. Given the limited scope of the studies, a more extensive validation of the various algorithms is clearly indicated.

The model used to calculate radiative fluxes is modified from Tsay et al. (1989), by replacing the discrete ordinate solution of the radiative transfer equation with a delta-Eddington two-stream approximation for shortwave calculations and a hemispheric mean two-stream approximation with an internal source function for longwave calculations (Toon et al. 1989). Gas absorption for water vapor, ozone, CO_2, and oxygen is parameterized using an exponential sum fitting technique with 24 bands at varying intervals without overlap for the shortwave region, and 9 bands at 200-cm^{-1} intervals including overlap of gases for the longwave region. Cloud single scattering properties are parameterized using the scheme of Slingo (1989):

$$\omega = c_1 + c_2 R_e$$

$$g = c_3 + c_4 R_e$$

$$\beta = (c_5 + c_6 / R_e)\text{LWC},$$

where ω, g, and β are the single-scattering albedo, the asymmetry factor, and the volume extinction coefficient, R_e is the effective radius, and LWC is the liquid water concentration. The constants c_i are determined by linear fits to results from Mie calculations for each spectral band over a range of cloud types. Clouds are represented as Mie scattering layers of variable thickness. Cloud height and optical thickness are set to the values reported in the ISCCP dataset. Cloud physical thickness is calculated from the above parameterization with an effective radius R_e of 10 μm and a liquid water concentration of 0.2 g m^{-3}. These values were chosen to be consistent with the ISCCP retrieval algorithm. During winter no cloud optical thickness is reported in the ISCCP dataset so the mean summer value of 10.5 was used instead. Optical depths for ice crystal clouds calculated by Curry et al. (1990) range from 5 to 21 in winter. The sensitivity of radiative fluxes to this assumption is tested in section 6b. Although cloud amount in seven categories is reported in the dataset, only total cloud amount is used in the analysis due to computational constraints. Monthly averages of cloud optical properties for total cloud amount contained in the ISCCP dataset are computed from the 3-h values of seven of the cloud types using an averaging scheme that accounts for the nonlinear relationship between cloud optical properties and their radiative effects (Rossow and Schiffer 1991). For each grid cell separate calculations are performed for cloud-free and cloudy conditions. Results are linearly averaged with the fractional area of cloud and clear sky as weights. This linear averaging, neglecting the effect of reflections from cloud sides and leakage of radiation through cloud walls, seems legitimate in the Arctic regions, where stratiform clouds dominate and cloudiness is generally high. Daily and month-to-month variation of solar zenith angle is treated by averaging calculations at 6-h intervals for the middle of the month. We found that using this integration step resulted in only a small error when compared with shorter (30-min) integration steps.

To calculate radiative fluxes, surface reflectivity and emissivity need to be specified for each of the spectral bands used in the radiative transfer scheme. Consistent with the ISCCP analysis, emissivity is assumed to be unity. Spectral albedos in the 24 bands must be estimated from the single channel reflectance (0.6 μm) reported in the C2 dataset. The problem is complicated by the fact that a variety of surface types may exist within each grid cell; the proper mixture must be determined before reflectances can be assigned. The surface types considered are: open water, melt ponds, bare ice, and snow-covered ice with either 300- or 1000-μm snow-grain size. The spectral albedos for these surfaces are in part extracted from the literature and in part computed using a four-stream model analogous to the development of Warren and Wiscombe (1980). For the modeled snow albedo, snow-grain size is season dependent. A soot content of 0.2 ppmw, consistent with the amounts necessary to match measured albedos by Grenfell and Maykut (1977), is used. The albedo at the lower boundary, the snow–ice interface, was set to the spectral albedo of ice from which the snow has been removed. The snow depth in the nonmelt season was assumed to be 40 cm, a value typical for early May. Spectra for melting first- and second-year ice, as well as melt ponds are taken from Grenfell and Maykut (1977).

With these temporal distributions of the surface types defined, and not allowing more than three in any given month, we assign the 24 reflectances by first determining what combination of surface types would produce the reported visible reflectance. Ice concentration data from the C2 dataset is used, thereby fixing two of the (possible) three types. The remaining spectral band albedos are assigned as the sum of the weighted "pure" reflectances in each band; that is $\mathbf{A} = \mathbf{SF}$, where $\mathbf{A}$ is the vector of albedos in the 24 bands, $\mathbf{S}$ is a matrix of pure spectral signatures for each surface type and each spectral band, and $\mathbf{F}$ is the five-element vector of the fractional coverage of each surface type. In practice the estimated melt pond fraction may assume unrealistic values so that the right-hand side of the above equation is adjusted for unmodeled effects.

One further addition to the information provided in the C2 data was necessary. The C2 dataset reports atmospheric temperatures at only four levels (five if a cloud is present) so that detail in the vertical temperature profile must be reconstructed. We drew on a dataset of atmospheric vapor and temperature profiles from North Polar drifting stations compiled by Serreze et al. (1992). The vertical resolution of the TOVS temperature and humidity profiles being too coarse to represent the radiatively important low-level inversion, the inversion statistics from this ice island dataset were used to add a climatological inversion to the ISCCP profiles. Similarly, information on water vapor and ozone abundance is only reported in integrated columnar quantities. Standard subarctic profiles were used to reconstruct water vapor and ozone profiles from the total columnar amounts by assuming a constant ratio of layer to column amounts.

4. Basinwide mean fluxes and cloud forcing

a. Surface

For the baseline case, calculations were conducted for all ocean areas north of 62.5°N. Only total cloudiness is considered. Total aerosol optical depth is set to 0.06 and does not vary with season or place. Surface fluxes from the baseline calculations are shown in Table 2 and Figs. 2 and 3, with symbols defined in Table 1.

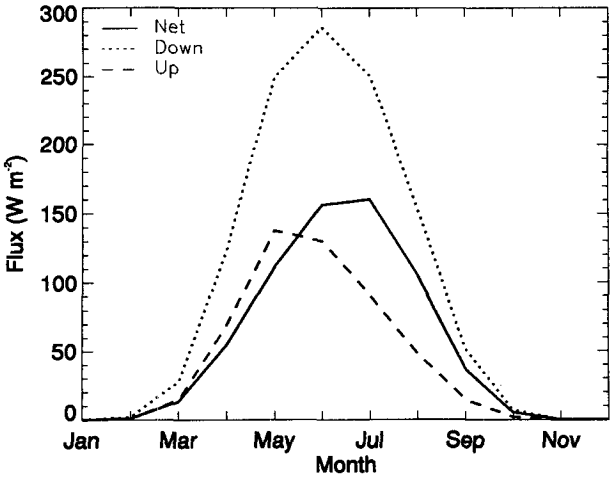

FIG. 2. Shortwave fluxes at the surface for all ocean areas north of 62.5°N.

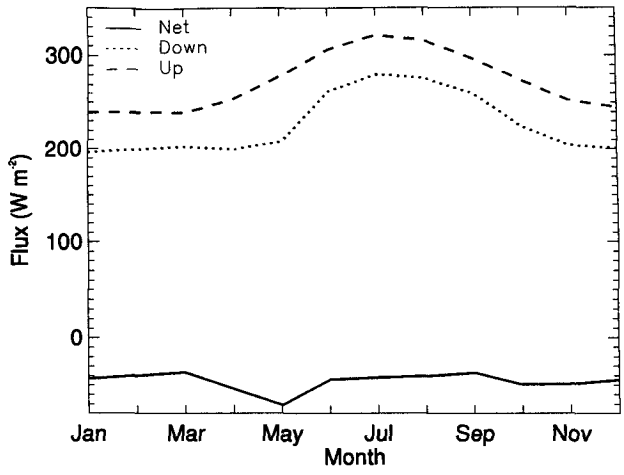

FIG. 3. Longwave fluxes at the surface for all ocean areas north of 62.5°N.

Downwelling shortwave radiation increases from February to a June maximum of 286 W m^{-2}. Downwelling longwave radiation during summer is of a similar magnitude but has a maximum of 279 W m^{-2} a month later in July. Variation in downwelling longwave radiation is small from November through May and the minimum occurs in April when air temperatures have begun to rise and cloud amount decreases from winter to spring. While incoming shortwave radiation increases and decreases monotonically to and from the June maximum, downwelling longwave radiation shows a rather abrupt jump of 55 W m^{-2} from May to June Net longwave fluxes are negative (loss from the surface) throughout the year. Maximum losses of −71 W m^{-2} occur during May when rising surface temperatures coincide with a minimum in cloudiness. Shortwave gains exceed longwave losses from April through September, and the net surface radiation balance varies from a minimum in November of −48 W m^{-2} to a maximum in July of 118 W m^{-2}. This maximum occurs one month after the maximum in downwelling shortwave radiation and is caused mainly by a drop in albedo during this time of the year.

To investigate the net radiative effect of clouds in the Arctic regions cloud forcings are determined. Cloud forcing is the integrated partial derivative of the radiative flux with respect to the cloud fraction and is defined as

$$\mathrm{CS}_s = \int_0^{A_c} \frac{\partial S_s}{\partial a}\, da = S_s(A_c) - S_s(0)$$

$$\mathrm{CF}_s = \int_0^{A_c} \frac{\partial F_s}{\partial a}\, da = F_s(A_c) - F_s(0)$$

$$\mathrm{CNET}_s = \mathrm{CS}_s + \mathrm{CF}_s,$$

where CS, CF, and CNET are the shortwave, longwave, and net cloud forcing for the surface (subscript s), A_c is the total cloud amount, S_s and F_s are the net short- and longwave fluxes at the surface, and a is cloud fraction. Cloud forcings are negative for cooling and positive for warming. The net cloud forcing is the sum of both cloud-forcing parameters. Cloud-forcing parameters were calculated for each individual grid cell and averaged spatially and over the eight years under investigation. Surface cloud forcings are shown in Fig. 4. During the winter season, clouds have a warming effect of about 66 W m^{-2} and the net cloud forcing at the surface remains positive from October through May. During summer the effect of clouds to decrease

TABLE 1. Symbol definitions. All flux variables are subscripted with s or t for surface or top of the atmosphere.

Variable	Description
$F\downarrow$	Downwelling longwave flux
$F\uparrow$	Upwelling longwave flux
F	Net longwave flux
R	Net flux (balance)
S	Net shortwave flux
$S\downarrow$	Downwelling shortwave flux
$S\downarrow_{\mathrm{dir}}$	Direct downwelling shortwave flux
$S\downarrow_{\mathrm{diff}}$	Diffuse downwelling shortwave flux
$S\uparrow$	Upwelling shortwave flux
CS	Shortwave cloud forcing
CF	Longwave cloud forcing
CNET	Net cloud forcing
A_c	Total cloud fraction
A_{marg}	Marginal cloud fraction
R_e	Effective cloud droplet radius
P_c	Cloud-top pressure
T_c	Cloud-top temperature
τ	Cloud optical depth
α	Spectrally and hemispherically integrated directional albedo
$r_{0.6}$	AVHRR channel 1 surface reflectance
r_s	Surface reflectance
T_s	Surface skin temperature

TABLE 2. Radiative fluxes (W m^{-2}) and cloud forcing for the ISCCP baseline case.

Month	Jan	Feb	Mar	Apr	May	Jun	Jul	Aug	Sep	Oct	Nov	Dec
A_c	0.7	0.7	0.6	0.5	0.5	0.5	0.5	0.6	0.6	0.7	0.6	0.7
α	0.0	0.1	0.6	0.6	0.5	0.4	0.4	0.3	0.3	0.3	0.00	0.00
$S\downarrow_t$	0	7	70	236	414	508	475	324	134	23	0	0
$S\uparrow_t$	0	5	47	152	252	267	236	164	73	14	0	0
S_t	0	2	23	84	162	240	239	160	60	9	0	0
$F\uparrow_t$	182	182	187	200	220	223	227	221	211	208	193	186
R_t	−182	−180	−164	−115	−57	17	12	−62	−151	−200	−193	−186
$S\downarrow_{dir,s}$	0	1	12	63	146	160	129	74	23	3	0	0
$S\downarrow_{diff,s}$	0	1	16	61	104	127	122	79	29	4	0	0
$S\downarrow_s$	0	2	28	124	250	287	251	153	52	7	0	0
$S\uparrow_s$	0	1	14	69	138	130	91	48	15	2	0	0
S_s	0	1	13	55	112	156	160	105	37	5	0	0
$F\downarrow_s$	196	199	202	1989	207	262	279	276	260	224	204	200
$F\uparrow_s$	239	239	238	253	278	306	321	316	297	274	252	245
F_s	−43	−40	−36	−54	−71	−44	−42	−40	−37	−49	−48	−44
R_s	−43	−39	−23	1	41	112	118	65	0	−44	−48	−44
CS_t	0	−2	−12	−31	−48	−70	−79	−61	−29	−6	0	0
CF_t	22	23	21	17	13	13	16	16	15	21	21	23
$CNET_t$	22	22	8	−14	−34	−57	−63	−45	−14	16	21	23
CS_s	0	−2	−13	−34	−53	−71	−78	−60	−29	−6	0	0
CF_s	66	68	71	59	60	30	31	35	40	72	65	66
$CNET_s$	66	66	58	25	−3	−41	−47	−25	11	66	65	66

incoming shortwave radiation outweighs their longwave radiative effects: clouds have a net cooling effect ranging from 4 W m^{-2} in April and May to a maximum of 47 W m^{-2} in July. These cloud forcings are in good agreement with those computed from a surface-based climatology (Curry and Ebert 1992).

b. *Top of atmosphere (TOA)*

Since radiation is the only form of energy exchange at the top of the atmosphere, radiative fluxes there provide a measure of the total energy balance of the earth. Net TOA shortwave radiation (Fig. 5) increases from February to June, from 2 to 240 W m^{-2}, respectively, and drops to 9 W m^{-2} in October. The maximum occurs in June. Even though incoming shortwave at the TOA decreases by 33 W m^{-2} from June to July, net TOA shortwave drops by only 1 W m^{-2} due to the effect of the drop in surface albedo on the TOA fluxes. This drop in surface albedo obviously outweighs the effect of an increase in cloudiness from June to July (Fig. 1), which is expected to increase the planetary albedo. Since there is no thermal input at the top of the atmosphere, the net longwave radiation balance at the top of the atmosphere is negative throughout the year. The TOA longwave flux remains almost constant (within 5 W m^{-2}) from December through March with a maximum of −182 W m^{-2} in January and a minimum of −223 W m^{-2} in June. Compared with the longwave fluxes at the surface, the annual variability at the top of the atmosphere is rather small. Except for the months of June and July when the net balance is

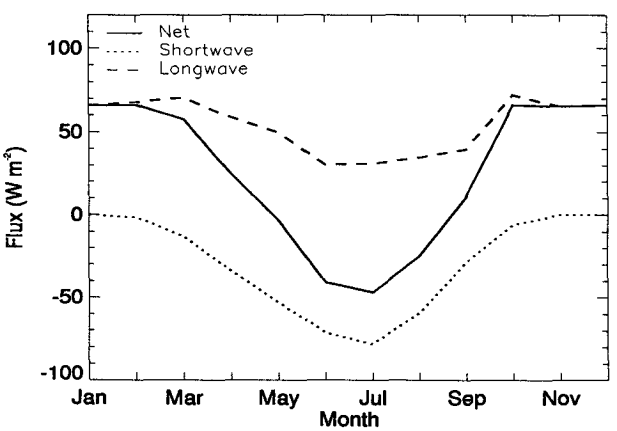

FIG. 4. Net, shortwave, and longwave cloud forcings at the surface.

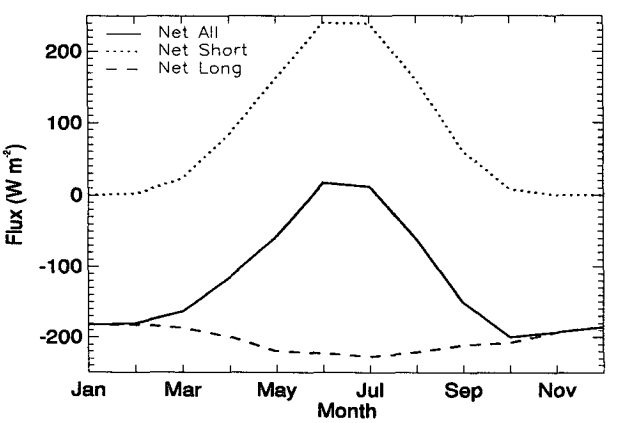

FIG. 5. Top-of-the-atmosphere fluxes.

slightly positive (17 and 12 W m^{-2}, respectively), the Arctic loses energy at its top boundary throughout the year. The maximum (−200 W m^{-2}) occurs in November. This radiative loss at the top of the atmosphere, which has to be balanced by energy exchange with lower latitudes and the lower boundary (the ice-covered ocean), is a major driving force in the global climate system (Nakamura and Oort 1988). In fact, our summer (June–July–August) average of −11 W m^{-2} is in close agreement with the −15 W m^{-2} value used by Nakamura and Oort. However, winter (December–January–February) losses of −183 W m^{-2} exceed their average (−157 W m^{-2}) by 26 W m^{-2}.

In the context of a CO_2 global warming scenario, which may or may not increase cloudiness, it is important to know the net radiative effects of clouds. Figure 6 shows the shortwave, longwave, and net cloud forcings at the top of the atmosphere. The impact of clouds on the longwave radiation balance is relatively small and shows little variation over the year. However, the effect of clouds on the shortwave radiation balance at the top of the atmosphere is significantly larger. In July at the maximum, the net effect of clouds on the total radiation balance is to reduce the energy input to the atmosphere by 79 W m^{-2}. A comparison with cloud forcings calculated for the surface (Fig. 4) shows that even though shortwave cloud forcings at the surface are almost identical to those at the top of the atmosphere, the net effect of clouds is greater at the surface during the winter and greater at the top of the atmosphere during the summer.

Unlike surface radiative fluxes, TOA radiative fluxes can only be obtained from satellite measurements or from modeling studies. A significant effort has been made to obtain TOA radiative fluxes from satellite (cf. Barkstrom et al. 1990; Ramanathan et al. 1989). Barkstrom et al. (1990) present zonal means from four months of ERBE data that overlap with the ISCCP dataset. Their results are compared with those computed from the ISCCP dataset in Fig. 7. Top-of-the-atmosphere fluxes calculated for the ISCCP baseline case are in excellent agreement with those measured by ERBE; the greatest difference is in October for shortwave values, where ISCCP values are 0 but ERBE measures 18 W m^{-2}. This difference is explained by the fact that no shortwave retrievals (and therefore no flux calculations) are performed beyond the solar zenith angle cutoff (72.5°). Barkstrom et al. (1990) estimate the accuracy of monthly averaged statistics at a regional scale as 6 W m^{-2}. Over the poles and snow-covered areas, where cloud detection is error prone, this accuracy is expected to be less (Ramanathan et al. 1989).

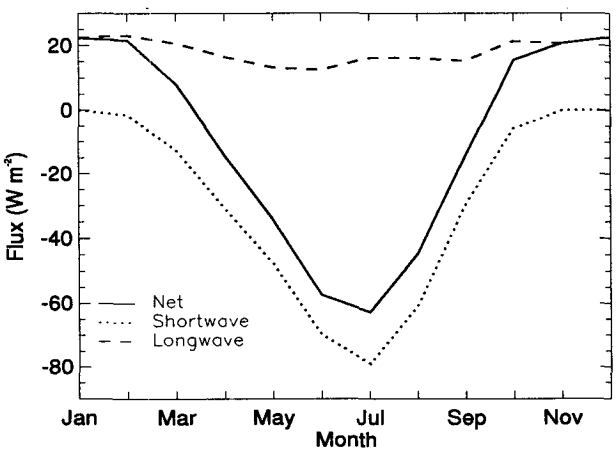

FIG. 6. Top-of-the-atmosphere cloud forcings.

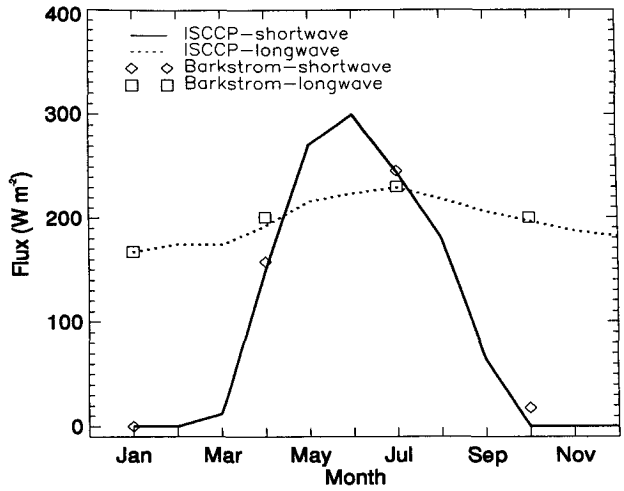

FIG. 7. Comparison of upwelling longwave and shortwave radiative fluxes from the ISCCP baseline case and ERBE data. ERBE data from Barkstrom et al. (1990; their Fig. 4 and 5) at 80°N. The period of comparison is January 1986, and April, July, October of 1985. ISCCP data plotted here represent the zonal mean of the ISCCP grid cells centered at 81.3°N.

Zonally averaged cloud forcings for regions north of 60° for 4 days in July 1985 have been calculated by Li and Leighton (1991). In their approach, an AVHRR-based algorithm for scene identification is applied to broadband ERBE radiances, to calculate outgoing longwave and shortwave fluxes. Figure 8 compares net cloud forcings calculated by Li and Leighton with those calculated for the ISCCP baseline case. The curves labeled "ERBE" and "ERBE with AVHRR" are the cloud forcings from the ERBE dataset and those computed from the ERBE dataset using an AVHRR-based scene identification, respectively. Li and Leighton stress the point that scene identification, which is more accurately accomplished using the higher-resolution, multichannel AVHRR sensor, is extremely important when calculating cloud forcings over the polar regions. The excellent agreement between the ISCCP calculated cloud forcings and those obtained from ERBE using the AVHRR scene identification is encouraging. The close agreement between

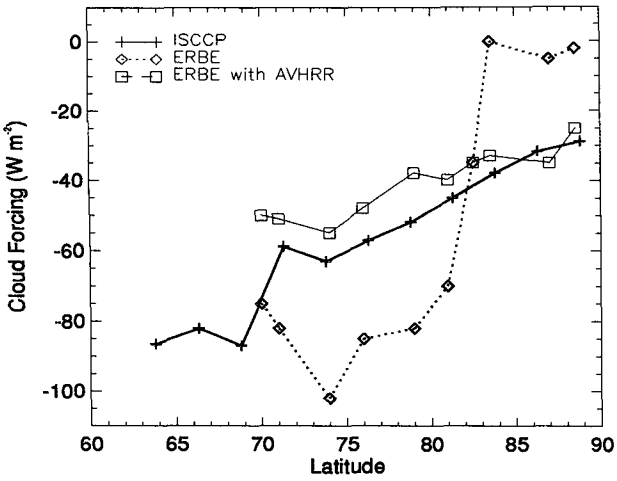

FIG. 8. Longitudinally averaged net cloud forcings at TOA calculated from the ISCCP dataset and measured by the ERBE instrument. "ERBE with AVHRR" are ERBE fluxes weighted by AVHRR-derived cloud fractions.

the two datasets further disputes the finding that net cloud forcings at the top of the arctic atmosphere are positive (Ramanathan et al. 1989). Indeed, the unmodified ERBE data show that annual net cloud forcings north of 80°N are positive. Given their calculated cloud forcing being close to zero near the pole in July, with positive winter values, it is apparent why Ramanathan et al. arrived at their conclusion about net cloud forcings in the Arctic.

5. Spatial variability of fluxes and cloud forcing

Spatial variability was also examined. Only spatial patterns for January and June are given here; a complete set (though for a shorter time period) can be found in Schweiger (1992). In March downwelling shortwave radiation at the surface in the central Arctic is 20–25 W m^{-2}, increasing southward. A modulation of the solar zenith angle effect by cloud amount is seen over the Greenland and Norwegian Seas, where cloudiness is usually greater than in other regions of the Arctic. In April this pattern persists, but downwelling fluxes have increased by about 100 W m^{-2} for the areas north of 70° with less of a latitudinal gradient than that in March. Since the ISCCP dataset reports fewer clouds in the central Arctic than elsewhere, in May this region receives more solar radiation (300 W m^{-2}) than other areas of the Arctic. The minimum again occurs over the Greenland and Norwegian Seas where cloud amounts are persistently high. In June (Fig. 9) and July, downwelling shortwave patterns vary little over most of the Arctic region with downwelling fluxes in the order of 300–325 W m^{-2} for the central Arctic and 180–280 W m^{-2} in the Norwegian Sea. A steep gradient can again be observed in the Greenland and Norwegian Seas as well as the Barents Sea, where summer cloud amounts of 80% reduce incoming shortwave radiation substantially. In these areas summer ice concentrations, and therefore areally averaged albedos, are lower. In August, the solar zenith angle–related concentric pattern redevelops and cloudiness has a secondary effect on the spatial distribution of shortwave fluxes.

Downwelling longwave fluxes show little variation over most of the Arctic and are on the order of 175 W m^{-2} from November through April. Results for January are shown in Fig. 10a. A strong increase up to 300 W m^{-2} can be found over the Norwegian, Greenland, and Barents Seas. This gradient is also fairly constant for these months and is again caused by the greater cloudiness over these areas. In May the peripheral seas, because of rising temperatures, begin to receive greater amounts of longwave radiation (200 W m^{-2}), while the central Arctic remains at the 175 W m^{-2} level. In June (Fig. 10b) a sudden jump to 250 W m^{-2} with little variation over the central areas occurs, and the maximum is reached in July with 275 W m^{-2} over most of the Arctic Ocean and the peripheral seas. In August this pattern persists at approximately the same level before values drop again most drastically in the central Arctic. The spatial distributions of net cloud forcing at the surface during January and June are shown in Figs. 11a and 11b. The relationship between the cloud forcing and downwelling shortwave and longwave radiation in Figs. 9 and 10 is readily apparent. For a more detailed discussion of the spatial variability see Schweiger (1992).

6. Sensitivity analyses

In this section the sensitivity of the computed fluxes to cloud amount, height, droplet size, and optical depth,

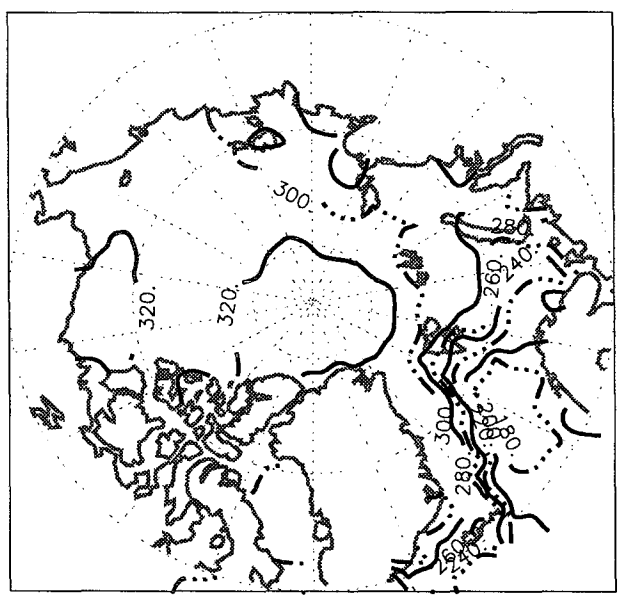

FIG. 9. The spatial distribution of downwelling shortwave radiation (W m^{-2}) during June.

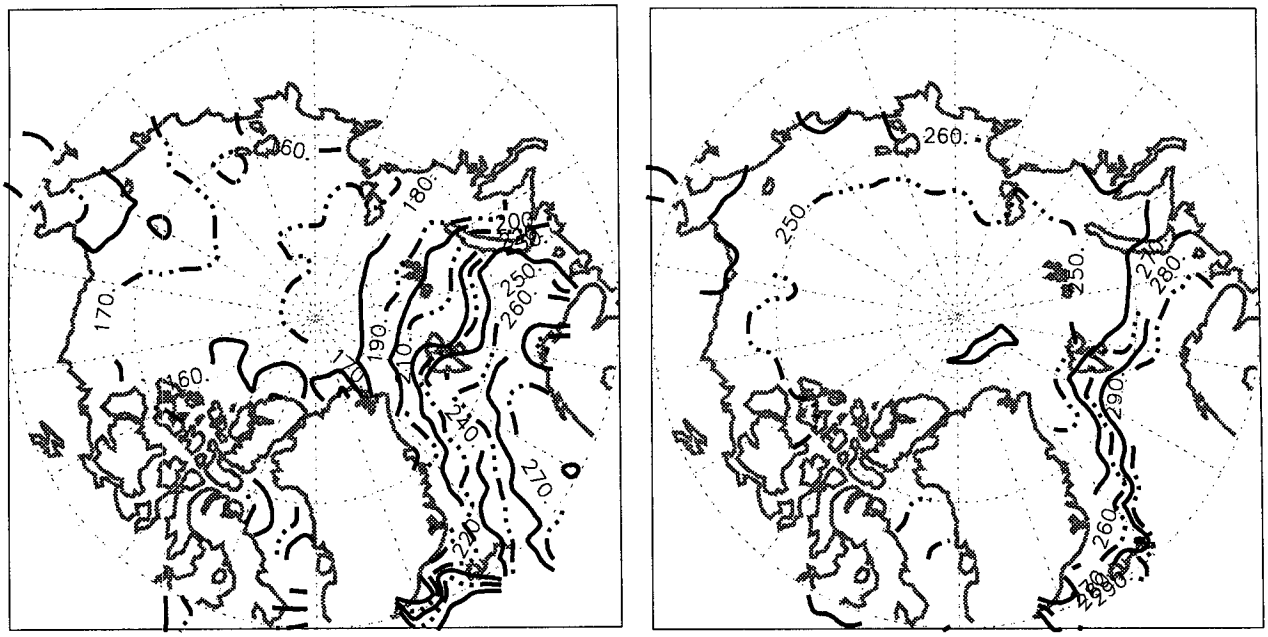

FIG. 10. The spatial distribution of downwelling longwave radiation (W m^{-2}) during (a) January and (b) June.

surface reflectance and temperature, and data time step are examined. The results are summarized in Table 3. In this and subsequent tables, the columns labeled "all" refer to the entire study area (ocean areas north of 62.5°N) and columns labeled ">75" refer to ocean areas north of 75°N. Where no particular mention is made of area, the results pertain to the entire study region.

a. Sensitivity to cloud amount

There is considerable uncertainty in reported cloud amounts in the Arctic (Schweiger and Key 1992). To evaluate the sensitivity of surface radiative fluxes to errors in the determination of cloud amount, two separate sensitivity studies were conducted. Categories "cloud amount" and "marginal" in Table 3 show the

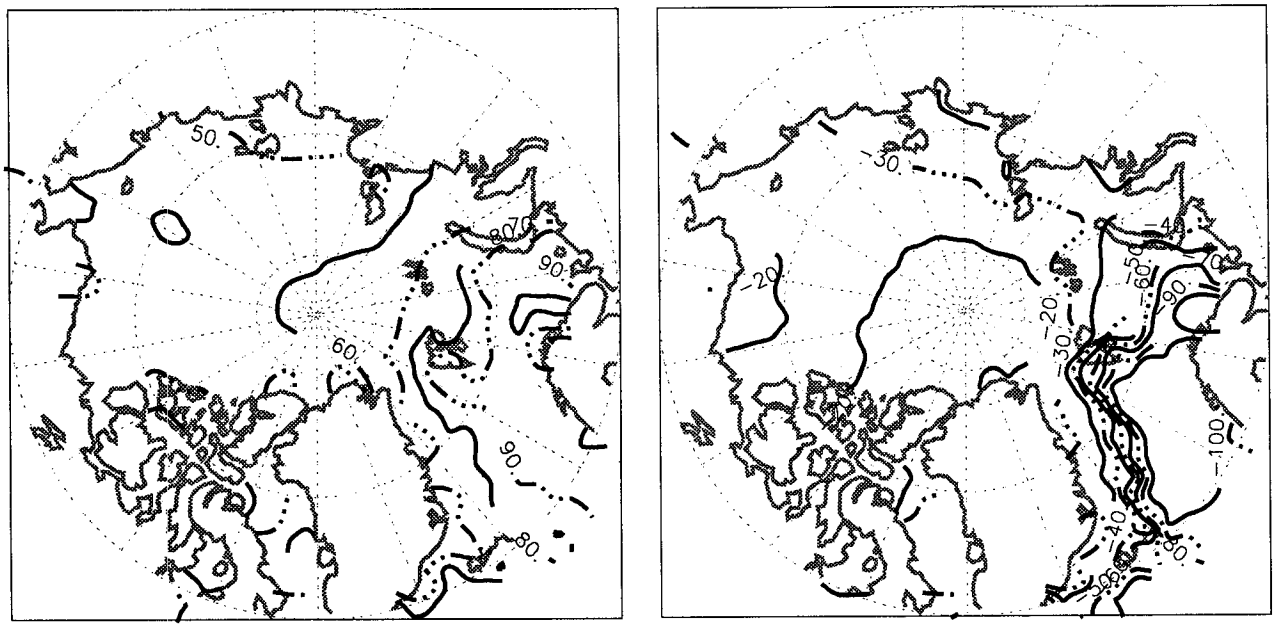

FIG. 11. The spatial distribution of surface net cloud forcing (W m^{-2}) during (a) January and (b) June.

TABLE 3. Sensitivity of surface fluxes to changes in cloud and surface parameters.

	Jan All $F\downarrow$	Jan All R	Jan >75 $F\downarrow$	Jan >75 R	Jul All $F\downarrow$	Jul All R	Jul All $S\downarrow$	Jul >75 $F\downarrow$	Jul >75 R	Jul >75 $S\downarrow$
Baseline case	206	−43	190	−40	280	127	259	267	113	275
Cloud amount										
−20%	192	−57	177	−52	274	137	279	263	129	291
+20%	220	−29	203	−26	284	118	240	272	106	258
Marginal cloud										
−	182	−59	164	−57	268	136	276	256	122	296
+	229	−27	216	−22	291	121	243	279	105	255
Cloud-top pressure										
−10%	206	−43	189	−40	278	126	259	266	112	274
+10%	221	−28	202	−27	283	131	259	270	115	275
Cloud-droplet radius										
5 μm	204	−45	188	−41	279	124	254	267	111	271
Surface reflectance										
−15%	—	—	—	—	—	138	255	—	128	270
+15%	—	—	—	—	—	116	262	—	98	280
Cloud optical depth										
−20%	205	−44	189	−40	279	132	266	267	117	281
+20%	207	−42	191	−38	280	123	253	268	110	270
Surface temperature										
−4 K	198	−35	183	−32	267	133	259	255	120	275
+4 K	214	−51	197	−47	292	121	259	280	107	275

results for comparison with the "baseline case." Values for the baseline case are different from those presented previously; they are averages for January and July of 1985 only. For the "cloud amount" sensitivity study, the cloud amount was varied upward and downward by 20% (relative) without altering any of the other parameters used in the radiative transfer calculations. In January a 20% increase in cloud amount causes an increase in downwelling longwave radiation of 14 W m^{-2} for the entire area and 13 W m^{-2} north of 75°N. In summer the effect on longwave fluxes is smaller, particularly north of 75°N, but the effect on shortwave fluxes is substantial and on the order of 20 W m^{-2}.

Since the accuracy of the ISCCP cloud detection algorithm will affect the accuracy of the retrieved cloud properties as well as surface temperature and surface reflectance, following Rossow et al. (1990), a study was conducted to determine the combined effect of errors in the cloud detection step of the ISCCP algorithm on the derived surface radiative fluxes. Marginal clouds and those potentially missed by the ISCCP cloud retrieval algorithm have properties that are different from those of detected clouds. The larger decision thresholds applied to the "certainly cloudy" pixels cause these pixels to have lower cloud-top temperatures and a greater cloud optical depth than marginal clouds. The retrieved surface properties are not independent of the decision thresholds applied in the cloud analysis. If undetected, the properties of these cloudy pixels will affect the statistics for the surface variables reflectance and temperature. Because of the photon-conservative nature of the ISCCP algorithm (i.e., radiation must come from either surface or cloud; if clouds are missed, radiation that is falsely attributed to the surface must actually have been radiated by the clouds), a new set of surface and cloud properties can be computed from information on the properties of marginally cloudy pixels. These are computed by removing the effect of marginal clouds (they are included in the total cloud amount) from the radiative properties reported in the ISCCP dataset:

$$T'_c = \frac{A_c T_c - A_{\text{marg}} T_{\text{marg}}}{A_c - A_{\text{marg}}}$$

$$T'_s = \frac{(1 - A_c) T_s + A_{\text{marg}} T_{\text{marg}}}{1 - A_c + A_{\text{marg}}}$$

$$\tau' = \frac{A_c \tau_c - A_{\text{marg}} \tau_{\text{marg}}}{A_c - A_{\text{marg}}}$$

$$r'_s = \frac{(1 - A_c) r_s + A_{\text{marg}} \tau_{\text{marg}}}{1 - A_c + A_{\text{marg}}},$$

where A_c and A_{marg} are the total and marginal cloud amounts, T_s and r_s refer to the surface temperature and surface reflectivity, T_c and τ_c are the cloud-top temperature and cloud optical depths for totally cloudy pixels, and T_{marg} and τ_{marg} are the cloud-top temper-

ature and cloud optical thickness for marginally cloudy pixels. The primed variables are calculated from the digital counts reported in the ISCCP dataset rather than from the geophysical variables. Since $\tau + r = 1$ in digital count coordinates, r'_s can be calculated using $-\tau_{\text{marg}}$ instead of r_{marg}, which is not reported. This set of new variables represents the assumption that the ISCCP algorithm actually overestimates cloud amount and that marginal clouds and their attributed radiative properties actually represent the surface. Previously presented evidence suggests, however, that the ISCCP cloud detection algorithm, at least during the summer months, underestimates "true" cloud amounts. The combined effect of the cloud amount underestimate on all ISCCP parameters is approximated by the assumption that changes in surface and cloud radiative properties due to changes in the decision thresholds are symmetric about the reported values. The magnitude of the effect of removing marginal "objects" from clouds and adding them to the surface is assumed to be equal to the effect (in the opposite direction) of clouds that were actually missed by the ISCCP algorithm. For radiative consistency, variables are calculated from the digital counts, rather than the geophysical variables.

Category "marginal cloud" in Table 3 reports the results of this sensitivity study. The row labeled "+" indicates the radiative fluxes that would be expected if "missed" clouds were actually included in the calculations and the above assumptions about the properties of these clouds were correct. The effect is to increase cloud amount. In this case January downwelling longwave fluxes for the entire area increase from 206 to 229 W m^{-2} and the net radiation balance increases from −43 to −27 W m^{-2}. In July downwelling longwave fluxes increase from 280 to 291 W m^{-2} and shortwave fluxes decrease from 259 to 243 W m^{-2} for the entire area; the net radiation balance is decreased by only 5 W m^{-2}. In order to compare the sensitivity of these radiative fluxes to those computed when cloud fraction alone was varied, it is important to consider that the addition of marginal clouds to the total cloud amounts increases total cloud amounts by (relative) 30% in January and 20% in July. For the "cloud amount" sensitivity study the cloud amount was increased (relative) by 20% for January and July.

Next, spatially averaged downwelling radiative fluxes calculated for ocean areas north of 75°N were compared with measured radiative fluxes reported by Marshunova. The comparison shows a good agreement of downwelling shortwave fluxes but a substantial disagreement in midsummer downwelling longwave fluxes. The following sensitivity study was conducted to test the hypothesis that the discrepancies in downwelling longwave fluxes are mainly caused by the fact that the ISCCP algorithm by design will miss a substantial fraction of thin low clouds. Figures 12 and 13 show a comparison of downwelling longwave and

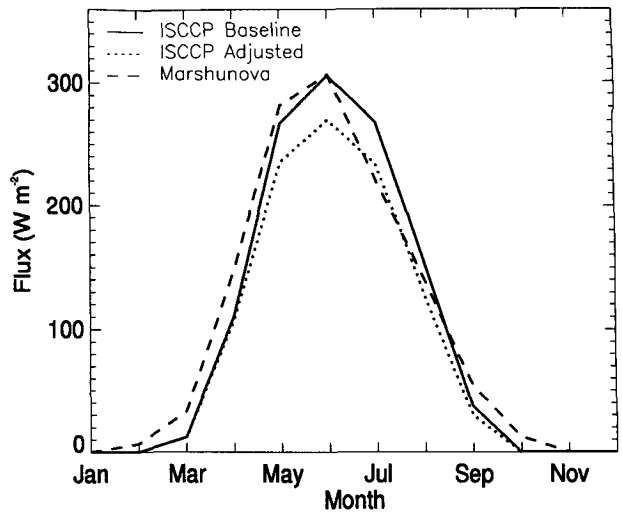

FIG. 12. Downwelling shortwave flux calculated from the ISCCP dataset, climatological values from Marshunova, and ISCCP values corrected for potentially underestimated cloud amounts.

shortwave radiative fluxes for the ISCCP baseline case, the ones reported by Marshunova, and a sensitivity study in which a combination of ISCCP data and the cloud climatology of Warren et al. (1986, 1988) was used. This combination was produced by assuming that the ISCCP data indeed represent an underestimate and that the difference between the ISCCP dataset and the WAR cloud climatology is accounted for by thin low stratus clouds. In the figures, "ISCCP Adjusted" was therefore computed by adding a thin stratus cloud of optical depth 2 with its cloud top in the inversion layer. Cloud amounts for this cloud type are calculated as the difference between the climatological cloud amount

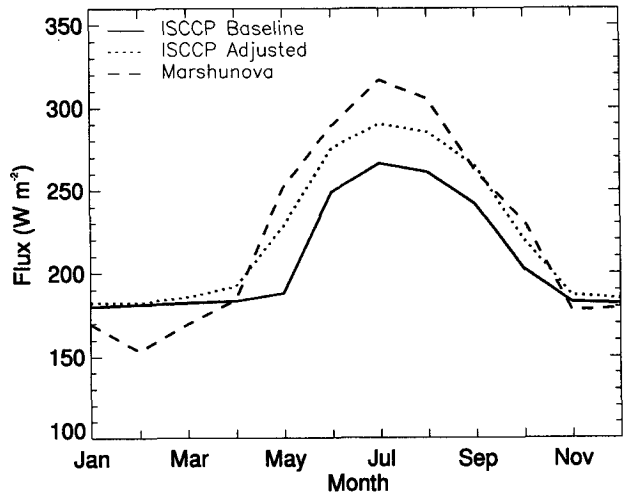

FIG. 13. Downwelling longwave flux calculated from the ISCCP dataset, climatological values from Marshunova, and ISCCP values corrected for potentially underestimated cloud amounts.

and the reported ISCCP cloud amount for each grid cell whenever the climatological cloud amount was greater. In cases where the climatological cloud amount was less than the ISCCP cloud amount (i.e., the central Arctic in winter), the ISCCP cloud amount was assumed to be correct. The comparison of downwelling longwave fluxes indicates that summer values are now substantially closer to those reported by Marshunova. July differences are now reduced to 25 W m^{-2}. In October (Fig. 13), downwelling longwave fluxes now exceed those reported by Marshunova. In spite of the small optical depth of the added clouds, the close match in downwelling shortwave fluxes between ISCCP calculated fluxes and those reported by Marshunova disappears in May and June. In July ISCCP shortwave fluxes are closer to Marshunova's, however. This sensitivity study indicates that not all of the differences encountered between the ISCCP and Marshunova datasets can be accounted for by the clouds missed by the ISCCP algorithm; other factors must be involved, and a combination of errors is likely. For example, if ISCCP surface reflectances were not underestimates as shown earlier (Schweiger et al. 1993), the effect of missed clouds on downwelling shortwave radiation would be smaller. It is also important to keep in mind that even though the WAR cloud climatology incorporates many of the data from Russian ice islands and drifting stations used by Marshunova, it spans a much longer record; interannual variability as well as measurement errors may account for some of the observed differences.

b. *Sensitivity to cloud height, droplet size, and optical depth*

The ISCCP dataset reports cloud-top height in pressure coordinates derived from the cloud-top temperature and the temperature profiles retrieved from the TOVS. The accuracy of the cloud-top height is therefore dependent on the accuracy of TOVS retrieval algorithms. In the approach selected for computation of surface radiative fluxes, the cloud-base height is computed from the optical depth and cloud-top height and is therefore affected by this error. To test the sensitivity of surface radiative fluxes to potential errors in cloud-top height, calculations were performed where cloud-top height (in pressure coordinates) was increased and decreased by 10%. The results are given in Table 3 under the category "cloud-top pressure." A 10% increase in cloud-top pressure in January causes an increase of 15 W m^{-2} in downwelling longwave radiation for the entire area. This increase is similar to the one expected from a 20% increase in cloud amount. In summer the effect of cloud height on downwelling longwave radiation is much smaller (3 W m^{-2}). Interestingly the effect of a 10% decrease in cloud-top pressure is very small (below rounding error) in January and only 2 W m^{-2} in July. Downwelling shortwave radiation shows little sensitivity to cloud-top height.

To determine the sensitivity of surface fluxes to assumptions about the effective radius of the cloud droplet distribution, a sensitivity study was conducted by calculating radiative fluxes for an effective radius of 5 μm instead of the 10 μm assumed for the baseline case. Because cloud physical thickness is calculated from optical depth under the assumption of a cloud microphysical model characterized by its effective droplet radius and liquid water content, a decrease in cloud-droplet size will cause a decrease in cloud physical thickness and thereby reduce downwelling longwave radiation. The sensitivity study conducted using a 5-μm cloud-droplet radius resulted in a small reduction in downwelling longwave radiation, by 2 W m^{-2}. Because of the effect of cloud-droplet size on cloud scattering properties and because of an increase in cloud height reducing multiple scattering effects between surface and clouds, downwelling shortwave fluxes are reduced by 5 W m^{-2}. Under the assumption that cloud optical depth is correctly retrieved, cloud microphysical parameters affect the calculation of surface fluxes very little compared with other variables. This agrees with the findings of Kergomard et al. (1993). Assumptions about cloud microphysical parameters in the radiative analysis step of the ISCCP algorithm do affect the accuracy of cloud optical depth values, however.

Virtually no information is available on the large-scale seasonal and spatial variability of cloud optical depths in the Arctic. Cloud optical depths measured from aircraft by Herman and Curry (1984) during the Arctic Stratus Experiment range between 2.1 and 24.3 for a spatially limited sample in June 1980. The accuracy of the optical depth retrieval in the ISCCP algorithm depends on the accuracy of the cloud detection step, the computation of surface reflectances, assumptions regarding gas absorption and cloud microphysical parameters, and general limitations with respect to the application of horizontally homogeneous plane-parallel radiative transfer theory. Over highly reflective surfaces the inversion of the radiative transfer equation is multivalued since a very thin cloud may result in the same top-of-the-atmosphere radiances as a thick cloud. In such cases, the ISCCP algorithm selects the greater optical depth. The same approach was selected by Kergomard et al. (1993) over ice-covered surfaces in the marginal ice zone. It is therefore likely that cloud optical depths reported by the ISCCP dataset are overestimates. A more accurate statement about the accuracy of cloud optical depths in the ISCCP dataset is currently not possible, however. A range of ±20% of the reported optical depths was selected to investigate the sensitivity of surface radiative fluxes to potential errors in the retrieved optical depth values. The effect of shortwave cloud optical depth on downwelling longwave fluxes again arises from the link between cloud optical depth and cloud physical thickness. The

TABLE 4. Measurement accuracies that result in a 5 W m^{-2} change in surface fluxes.

	Jan All $F\downarrow$	Jan All R	Jan >75 $F\downarrow$	Jan >75 R	Jul All $F\downarrow$	Jul All R	Jul All $S\downarrow$	Jul >75 $F\downarrow$	Jul >75 R	Jul >75 $S\downarrow$
Cloud amount	7%	7%	8%	8%	20%	10%	5%	22%	9%	6%
Cloud-top pressure	6%	7%	8%	8%	20%	20%	—	20%	33%	100%
Cloud-droplet radius	125%	125%	25%	250%	250%	80%	50%	—	125%	60%
Surface reflectance	—	—	—	—	—	7%	21%	—	5%	15%
Cloud optical depth	100%	100%	100%	100%	200%	22%	15%	200%	29%	18%
Surface temperature	1%	1%	1%	1%	1%	1%	1%	1%	1%	1%

increase in downwelling longwave fluxes due to a 20% increase in cloud optical depth amounts to only 1 W m^{-2} in January, smaller than the rounding error in July. The downwelling shortwave radiation then is reduced by 6 W m^{-2}, however.

c. *Sensitivity to surface reflectance and temperature*

The comparison of surface albedos calculated from the ISCCP dataset and from other datasets indicated that the surface reflectances reported in the ISCCP dataset are underestimates. The effect of incorrectly retrieved AVHRR channel 1 (0.6 μm) retrieved reflectances on the calculation of surface radiative fluxes is estimated to increase the surface reflectances by 15% (relative to the observed values). A 15% increase in surface reflectance (similar to the expected underestimate) despite an increase in downwelling shortwave radiation of 3 W m^{-2} will reduce the net radiation balance by 11 W m^{-2} when averaged over the entire study area. This decrease in net radiation is even greater (15 W m^{-2}) at latitudes north of 75°N even though it is accompanied by gains in downwelling shortwave of 5 W m^{-2} due to an increase in multiple reflections between clouds and surface.

ISCCP surface temperatures during winter probably represent overestimates, most likely due to the radiative effects of undetected ice crystal precipitation, which occurs frequently during the arctic winter (Ohtake et al. 1982). Through comparison with buoy data the difference between January mean temperatures and ISCCP surface temperatures is estimated to be about 4 K (Schweiger 1992), even though buoy data may in themselves be overestimates. A 4-K range about the baseline case was therefore selected to determine the sensitivity of surface radiative fluxes to potential errors in retrieved surface temperatures. In January a 4-K decrease in surface skin temperature results in an 8 W m^{-2} increase in net radiation and a decrease in downwelling longwave radiation of 8 W m^{-2}. This drop in downwelling longwave radiation is due to the fact that surface temperature is used in the construction of the temperature profile. A drop in surface temperature will cause a simultaneous drop in atmospheric temperatures below the height of the climatological inversion. In July the effect of surface temperature on downwelling longwave radiation is even greater (13 W m^{-2}) and the increase in net radiation is smaller (6 W m^{-2}).

As described previously, atmospheric temperature profiles provided by the TOVS in the ISCCP data stream do not provide sufficient vertical resolution to represent a surface inversion. A procedure was therefore developed to "retrofit" the TOVS profiles with a climatological inversion based on statistics compiled by Serreze et al. (1992). Using the TOVS profiles in the data stream without a retrofitted inversion decreases downwelling shortwave fluxes by 19 W m^{-2} from 208 to 189 W m^{-2} in January when averaged over the entire ISCCP period. In July the absence of a climatological surface inversion lowers the downwelling longwave fluxes by only 6 W m^{-2}.

With what accuracy do we need to measure cloud and surface characteristics to obtain useful flux estimates? This certainly depends on the application, but we can begin to answer the question by examining the accuracy with which the parameters must be measured in order to obtain a given change in the radiation balance. Table 4 shows the relative error in a particular input parameter that will cause a change of 5 W m^{-2} in the estimates of net and downwelling radiation at the surface. The values in the table are based on the sensitivities given in Table 3, and therefore are only applicable for the same conditions. As an example, to achieve a 5 W m^{-2} accuracy in the net radiation balance (R) in July over the entire Arctic basin we need to measure cloud amount to within 10%, assuming that all other parameters are measured perfectly. In light of the uncertainties in the ISCCP dataset, we conclude that a 5 W m^{-2} accuracy is not currently achievable.

d. *Temporal sensitivity: Monthly data versus 3-h data*

The ISCCP C2 dataset is a monthly average of the 3-h C1 dataset. All variables in the C2 set are simple linear averages of the 3-h data except for optical depth. Cloud optical depth is averaged in an "energy-weighted" fashion (Rossow and Schiffer 1991) to account for the nonlinear relationship between cloud op-

tical thickness and its radiative effect (cloud-top albedo). Since this energy-weighted averaging scheme is an approximation, a sensitivity study was conducted to investigate the accuracy of this nonlinear averaging scheme. Cloud fractions and optical depths for July 1985 were extracted from the C1 dataset and monthly average surface fluxes were computed for three grid cells by averaging 3-h fluxes. The C2 monthly averages of all other input variables were used in this study. While downwelling longwave fluxes show no sensitivity to the averaging scheme, downwelling shortwave fluxes calculated from the monthly averaged ISCCP C2 data are slightly higher than those calculated from the C1 dataset. This difference in downwelling shortwave is 7 W m^{-2} for the most southern location and 4 W m^{-2} for the most northern location. When cloud amounts are fixed at 60% and only optical depth is compared, monthly averages from the C1 and C2 datasets are in very close agreement. Considering the magnitude of other potential errors previously identified, this error can be considered small and the use of monthly data for the calculation of radiative fluxes seems clearly justified.

e. *Comparison of sensitivities*

In future development and refinement of arctic cloud detection algorithms and schemes to compute surface radiative fluxes from remote sensing platforms, it is desirable to order the identified sensitivities by their magnitude. To have such an ordered list would allow the prioritizing of research projects dealing with the improvement of the accuracy of any of the input variables. Following Ebert and Curry (1993) sensitivity parameters were computed as the scaled partial derivatives of surface radiative fluxes with respect to the input variables in the radiative transfer calculations:

$$\delta_F(\phi) = \frac{|\langle \phi_{\text{base}} \rangle|}{\langle F_{\text{base}} \rangle} \left\langle \frac{\partial F}{\partial \phi} \right\rangle,$$

where F is a flux density (downwelling longwave, shortwave, and net radiation), angle brackets denotes the mean over all grid cells, the subscript "base" denotes the baseline case value, and ϕ refers to the input variable that is changed in the sensitivity study. The partial derivatives are approximated by differencing over the range selected for the sensitivity study. The sensitivity parameters are scaled by the magnitude of their baseline case means in order to make them comparable to each other. Table 5 shows the sensitivity parameters calculated for the variables over the ranges shown in Table 3. Columns 1 and 2 present the sensitivity parameters for January and July averaged over the entire study area; column 3 presents the July results over areas that are 100% ice covered. Surface net radiation generally displays the greatest sensitivity to an error in the input variables. The largest sensitivities for net radiation are found in response to changes in cloud amount (1.91) and surface temperature (−1.50) in winter. The effect of cloud amount on net radiation is smaller in both January (1.55) and July (−0.30) when other variables are adjusted for the error introduced by missed clouds. In winter this occurs because an increase in cloud amount, and the associated increase in downwelling radiation, is accompanied by an increase in surface temperature (if missed clouds are colder than the surface), thereby reducing the sensitivity of net radiation to cloud amount. With respect to downwelling longwave radiation, the sensitivity to cloud amount is greater when adjustments to other variables are made. This greater sensitivity is related to the fact that in our model downwelling longwave radiation increases with an increase in surface temperature. Downwelling shortwave radiation is less sensitive to cloud amount when surface reflectivity and optical depth are adjusted to account for the error in these variables associated with the cloud amount underestimate. This is expected because an increase in cloud amount will reduce the optical depth; missed clouds are expected to have lower optical depths than those detected by the ISCCP algorithm. In July net radiation is most sensitive to changes in surface reflectance (0.66) and is twice this value (−1.26) when only completely ice-covered areas are considered.

Cloud-top pressure affects net radiation considerably in winter (0.98) but is less of a factor in summer (0.1). Cloud-droplet radius and cloud optical depth have a

TABLE 5. Relative sensitivity parameters.

	January All data	July All data	July Ice concentration = 100%
Longwave			
T_s*	0.30	0.14	0.14
P_c	0.35	0.09	0.06
A_c	0.34	0.09	0.07
$A_{c(adj)}$	0.41	0.20	0.12
R_e	0.02	0.00	0.00
τ	0.03	0.00	0.00
Net			
T_s	−1.50	−0.16	−0.19
P_c	0.98	0.10	0.08
A_c	1.91	−0.38	−0.23
$A_{c(adj)}$	1.55	−0.30	−0.31
R_e	0.18	0.05	0.04
$r_{0.6}$	—	−0.66	−1.26
τ	0.20	−0.18	−0.12
Shortwave			
P_c	—	0.00	0.00
A_c	—	−0.44	−0.25
$A_{c(adj)}$	—	−0.37	−0.22
R_e	—	0.04	0.03
$r_{0.6}$	—	0.09	0.14
τ	—	−0.14	−0.08

* For temperature the sensitivity parameter was scaled using the range in temperature rather than the mean baseline case temperature.

much smaller impact when compared with other input variables. Downwelling longwave radiation in winter is most significantly affected by cloud-top pressure (0.35), but cloud amount and surface temperature each affect downwelling longwave radiation with a similar magnitude. As noted before, the strong sensitivity of downwelling longwave radiation to surface temperature arises from the fact that ISCCP surface temperatures are used in the construction of temperature profiles. In summer the sensitivity to surface temperature even exceeds the sensitivity to cloud amount. Downwelling shortwave radiation is most significantly affected by cloud amount, followed by optical depth and surface reflectance. When only completely ice-covered surfaces are considered, the sensitivity of downwelling shortwave to surface reflectance is increased, due to the greater importance of multiple reflections between cloud bottom and surface.

7. Summary and conclusions

Radiative fluxes and cloud forcings for the ocean areas of the Arctic have been computed from the ISCCP C2 dataset. Spatially averaged shortwave fluxes agree well with climatological values. Downwelling longwave fluxes are significantly lower, largely because ISCCP cloud amounts are underestimates. Top of the atmosphere radiative fluxes are in excellent agreement with measurements from the ERBE instrument. Computed cloud forcings indicate that clouds have a warming effect both at the surface and the top of the atmosphere during winter and a cooling effect during summer. The net radiative effect of clouds during winter is greater at the surface whereas in summer the effect is greater at the top of the atmosphere. Over the annual cycle the net radiative effect of clouds at the top of the arctic atmosphere is one of cooling. This finding disputes a previous result from ERBE data that arctic clouds have a net warming effect (TOA).

Given the probable shortcomings of the ISCCP C2 cloud data product in the Arctic, it may be argued that radiative fluxes cannot be computed from this dataset with any useful degree of accuracy. The following counterarguments can be made: 1) Datasets and methodologies currently used to compute radiative forcing fields in sea-ice modeling experiments suffer from even greater shortcomings. Forcing fields such as those computed here, in spite of their potential inaccuracies and biases, should capture the spatial and temporal variability. A time series of sufficient length with simultaneous Arctic-wide coverage can only be established using satellite data. 2) The analysis presented here should provide valuable feedback to the research community involved in improving algorithms and defining new approaches to calculating radiative fluxes at the arctic surface. It is our belief that improvements in datasets such as the ISCCP's will depend on feedback by users and thus will occur in cycles of reprocessing and revalidation. In fact, a new "polar algorithm" is currently being prepared (W. Rossow 1993, personal communication). 3) Having established the general methodology and models, new datasets can be easily reprocessed and compared with previous versions of radiative flux fields. 4) Using a radiative transfer approach in conjunction with actual data, radiative forcing fields can be computed that allow more detailed studies of the sensitivity of sea ice models to radiative forcings than would be possible with simple parameterizations.

Sensitivities to errors in input parameters are generally greater during winter, with cloud amount being the most important parameter. During summer the surface radiation balance is most sensitive to errors in the measurements of surface reflectance. The retrieval of clouds, and hence of surface characteristics, will be significantly improved in the "next generation" ISCCP algorithm currently under development. This algorithm incorporates AVHRR channel 3 (3.7 μm) data, which has been shown to allow a better discrimination of some lower cloud types over ice- and snow-covered surfaces (e.g., Raschke et al. 1992; Key and Barry 1989).

While overall the results are encouraging, from the perspective of climate change detection the estimated potential error in net radiative fluxes at the surface of 20 W m^{-2} is too large. Estimates of the net radiative warming effect due to a doubling of CO_2 are on the order of 4 W m^{-2}. On the other hand, it is difficult to determine the accuracy of our satellite-based fluxes from the in situ data that is currently available. The development of improved algorithms for the retrieval of surface radiative properties should therefore be accompanied by the simultaneous development of validation datasets. These validation datasets should not consist of single point measurements but must somehow address the variability over scales that are compatible with satellite analyses.

Acknowledgments. This work was supported by NASA Grants NAGW-2407 and NAGW-2158. Thanks are due to W. Rossow for many useful discussions and to J. Curry and J. Francis for comments on an earlier draft of this paper.

REFERENCES

Barkstrom, B. R., E. F. Harrison, and R. B. Lee, 1990: Earth Radiation Budget Experiment: Preliminary seasonal results. *Eos,* **71,** 279.

Colony, R. L., I. Appel, and I. Rigor, 1992: Surface air temperature observations in the Arctic Basin. Applied Physics Laboratory, University of Washington. Tech. Memo. APL-UW TM, in press.

Curry, J. A., and E. E. Ebert, 1992: Annual cycle of radiation fluxes over the Arctic Ocean: Sensitivity to cloud optical properties. *J. Climate,* **5,** 1267–1278.

——, F. G. Meyer, L. F. Radke, C. A. Brock, and E. E. Ebert, 1990: Occurrence and characteristics of lower tropospheric ice crystal in the Arctic. *Int. J. Climatol.,* **10,** 749–764.

Deutsches Hydrographisches Institut, 1950: *Atlas der Eisverhältnisse des Nordatlantischen Ozean und Übersichtskarten der Eisver-*

hältnisse des Nord-und Südpolargebietes. Deutsches Hydrographisches Institut, 24 pp.

Ebert, E., and J. A. Curry, 1993: An intermediate one-dimensional thermodynamic sea ice model for investigating ice–atmosphere interactions. *J. Geophys. Res.*, **98**(C6), 10 085–10 109.

Fletcher, J. O., 1966: The arctic heat budget and atmospheric circulation. *Proc. Symp. Arctic Heat Budget and Atmospheric Circulation.* Memo. RM-5233-NSF, Rand Corp, 23–43. [Available from Rand Corporation, 1700 Main St., Santa Monica, CA 90406.]

Gavrilova, M. K., 1966: *Radiation Climate of the Arctic* (in Russian). Hydrometeorological Publishing House, 178 pp.

Grenfell, T. C., and G. A. Maykut, 1977: The optical properties of ice and snow in the Arctic basin. *J. Glaciol.*, **18,** 445–463.

Herman, G. F., and J. A. Curry, 1984: Observational and theoretical studies of solar radiation in Arctic stratus clouds. *J. Climate. Appl. Meteor.*, **23,** 5–24.

Kergomard, C., B. Bonnela, and Y. Fouquart, 1993: Retrieval of surface radiative fluxes on the marginal zone of sea ice from operational satellite data. *Ann. Glaciol.*, **17,** 201–206.

Key, J., and R. G. Barry, 1989: Cloud cover analysis with Arctic AVHRR data. 1. Cloud detection. *J. Geophys. Res.*, **94,** 18 521–18 535.

Larson, P., and S. Orvig, 1962: Albedo of Arctic surfaces. Publications in Meteorology, Vol. 54, McGill University, Montreal, 33 pp.

Li, Z., and H. G. Leighton, 1991: Scene identification and its effect on cloud radiative forcing in the Arctic. *J. Geophys. Res.*, **96,** 9175–9188.

Makshtas, A. P., 1991: The heat budget of Arctic ice in the winter. *International Glaciological Society Monograph,* International Glaciological Society, 77.

Marshunova, M. S., 1961: Principle regularities of the radiation balance of the underlying surface and of the atmosphere in the Arctic (in Russian). Tr. Arct. Antarct. Nauchno-Issled. Inst., 229, 5, Transl. by Rand Corp., Memo. RM-5003-PR, 51–103.

——, and N. T. Chernigovsky, 1966: Numerical characteristics of the radiation regime in the Soviet Arctic. Proc. Symp. Arctic Heat Budget and Atmospheric Circulation. Rand Corp. Memo., RM-5233-NFS, 281–297.

Nakamura, N., and A. H. Oort, 1988: Atmospheric heat budgets of the polar regions. *J. Geophys. Res.*, **93**(D8), 9510–9524.

Ohmura, A., 1981: Climate and energy balance of arctic tundra. *Zürcher Geographische Schriften,* **3,** 448.

——, and H. Gilgen, 1991: Global Energy Balance Archive GEBA. Report 2: The GEBA database, interactive applications, retrieving data. Internal Report, 66 pp. [Available from Department of Geography, ETH-Zürich, Winterthurerstrasse 190, CH-8057 Zürich, Switzerland.]

Ohtake, T., K. Jayaweera, and K. I. Sakurai, 1982: Observations of ice crystal formation in the lower Arctic atmosphere. *J. Atmos. Sci.*, **30,** 2898–2904.

Ramanathan, V., R. D. Cess, E. F. Harrison, P. Minnis, B. R. Barkstrom, E. Ahmad, and D. Hartmann, 1989: Cloud-radiative forcing and climate. Results for the Earth Radiation Budget Experiment. *Science,* **243,** 138–140.

Raschke, E., P. Bauer, and H. J. Lutz, 1992: Remote sensing in the polar regions. *Int. J. Remote Sens.*, **1,** 23–35.

Rossow, B. W., and A. A. Lacis, 1990: Global, seasonal cloud variations from satellite radiance measurements. Part II: Cloud properties and radiative effects. *J. Climate,* **3,** 1204–1253.

——, and R. A. Schiffer, 1991: ISCCP cloud data products. *Bull. Amer. Meteor. Soc.*, **72**(1), 2–20.

——, Y. Zhang, and A. A. Lacis, 1990: Calculations of atmospheric radiative flux profiles. *Proc. Seventh Conf. on Atmospheric Radiation.* San Francisco, Amer. Meteor. Soc.

——, L. C. Gardner, P. Lu, and A. Walker, 1991: International Satellite Cloud Climatology Project (ISCCP) documentation of cloud data. World Climate Research Programme, WMO/TD-No. 266.

Schmetz, J., 1989: Towards a surface radiation climatology. Retrieval of downward irradiances from Satellites. *Atmos. Res.*, **23,** 287–321.

Schweiger, J. A., 1992: Arctic radiative fluxes modeled from the ISCCP-C2 data set, 1983–1986. Ph.D. dissertation, University of Colorado, Boulder, 218 pp. [Available from Department of Geography, University of Colorado, Boulder, CO 80309.]

——, and J. Key, 1992: Arctic cloudiness: Comparison of ISCCP-C2 and *Nimbus-7* satellite-derived cloud products with a surface-based cloud climatology. *J. Climate,* **5,** 1514–1527.

——, M. C. Serreze, and J. Key, 1993: Arctic sea ice albedo: A comparison of two satellite-derived data sets. *Geophys. Res. Lett.*, **20**(1), 41–44.

Serreze, M. C., J. D. Kahl, and R. C. Schnell, 1992: Low-level temperature inversions of the Eurasian Arctic and comparisons with Soviet drifting station data. *J. Climate,* **5,** 615–630.

Slingo, A., 1989: A GCM parameterization for the shortwave radiative properties of water clouds. *J. Atmos. Sci.*, **46,** 1419–1427.

Stamnes, K. S., S. C. Tsay, W. Wiscombe, and K. Jayaweera, 1988: Numerical stable algorithms for discrete-ordinate-method radiative transfer in multiple scattering and emitting layered media. *Appl. Opt.*, **27,** 2502–2509.

Stuhlmann, R., and P. Bauer, 1991: Retrievals of surface radiation from satellite data and aircraft measurements over the polar regions. Report on polar radiation fluxes and sea-ice modeling. World Climate Research Programme, WCRP-62 WMO/TD-No 422, 29–40. [Available from Joint Planning Staff for WCRP, c/o WMO, Case Postale No. 2300, CH-1211 Geneva 20, Switzerland.]

Toon, O. B., C. P. McKay, and T. P. Ackerman, 1989: Rapid calculation of radiative heating rates and photo-dissociation rates in inhomogeneous multiple scattering atmospheres. *J. Geophys. Res.*, **94**(D13), 16 287–16 301.

Tsay, S. C., K. Stamnes, and K. Jayaweera, 1989: Radiative energy budget in the cloudy and hazy Arctic. *J. Atmos. Sci.*, **46,** 1002–1018.

Vowinckel, E., and S. Orvig, 1962: Insolation and absorbed solar radiation at the ground in the Arctic. *Publications in Meteorology,* No. 53, McGill University, Montreal, 32 pp. [Available from Department of Meteorology, McGill University, 805 Sherbrooke St. W., Montreal, Quebec H3A 2K6.]

——, and ——, 1963: Long wave radiation and total radiation balance at the surface in the Arctic. *Publications in Meteorology,* No. 62, McGill University, Montreal, 33 pp. [Available from Department of Meteorology, McGill University, 805 Sherbrooke St. W., Montreal, Quebec H3A 2K6.]

——, and ——, 1964: Radiation balance of the troposphere and of the earth-atmosphere system in the Arctic. *Publications in Meteorology,* No. 63, McGill University, Montreal, 23 pp. [Available from Department of Meteorology, McGill University, 805 Sherbrooke St. W., Montreal, Quebec H3A 2K6.]

Warren, S. G., and W. J. Wiscombe, 1980: A model for the spectral albedo of snow II. Snow containing atmospheric aerosols. *J. Atmos. Sci.*, **37,** 2734–2745.

——, C. J. Hahn, J. London, R. M. Chervin, and R. Jenne, 1986: Global distribution of total cloud cover and cloud type amounts over land. NCAR Tech. Note Tn-273+STR, Boulder, CO, 29 pp. [Available from National Center for Atmospheric Research, Boulder, CO 80307.]

——, ——, ——, ——, and ——, 1988: Global distribution of total cloud cover and cloud type amounts over the ocean. NCAR Tech. Note TN-317+STR, Boulder, CO, 41 pp. [Available from National Center for Atmospheric Research, Boulder, CO 80307.]

WMO, 1992: Report on the Workshop on Polar Radiation Fluxes and Sea-Ice Modelling. World Climate Research Programme. WMO/TD No. 442, Bremerhaven, Germany, 20 pp. [Available from Joint Planning Staff for WCRP, c/o WMO, Case Postale No. 2300, CH-1211 Geneva 20, Switzerland.]

U.S. Navy, 1958. *Hydrographic Office, Oceanographic Atlas of the Polar Seas, 1958.* U.S. Navy, 143 pp.